Heritage Science

RESEARCH

Open Access

The atypical hues of the Santa Cruz blue-and-white cargo: non-invasive analysis of glaze defects and color variations in mid-Ming porcelain

Ellen Hsieh[1*], Christian Fischer[2] and Bobby C. Orillaneda[3]

Abstract

Color variations and sometimes the frosted appearance of Chinese blue-and-white porcelain produced in folk kilns and recovered in underwater archaeological contexts are usually reported without further investigation. This study focuses on the causes responsible for the appearance of the glaze and blue decorations of late fifteenth-century blue-and-white porcelain from the Santa Cruz, one of the most important mid-Ming shipwrecks discovered in Asian waters. Besides detailed visual observations, chemical composition and colorimetric data were collected on a set of similarly shaped plates showing significant differences in the aspect of the glaze and tones and shades of the blue color. Results from portable X-ray fluorescence (pXRF) analysis confirmed the Jingdezhen origin of the ware and the use of domestic asbolane ores for the Co-based blue pigment. Visual and microstructural analysis has shown that the degree of opacity of the glaze is primarily linked to the crystallization of anorthite, which in some cases has pushed the pigment layer towards the surface, contributing to the development of white-brownish weathering spots. The colorimetric data acquired with fiber optics reflectance spectroscopy (FORS) allowed us to quantify chromaticity parameters and confirm the visual perception of a 'not-so-blue' color of the decoration. Without excluding a possible contribution of the underwater environment, the observed variations can be mainly attributed to the ware's production and more specifically to pigment characteristics, manufacturing processes, and firing conditions even though the connection with these factors is not straightforward and prompts further research and broader discussions. From a historical perspective, it is suggested that the atypical hues are correlated with the progressive switch from foreign to domestic pigment sources during the Chenghua period (1465–87 CE) and the subsequent technological adaptations required by an ever-increasing demand for Chinese blue-and-white porcelain at the turn of the sixteenth century.

Keywords Santa Cruz shipwreck, Blue-and-white porcelain, Jingdezhen, pXRF, FORS, Cobalt blue, Color

*Correspondence:
Ellen Hsieh
ehsieh@mx.nthu.edu.tw
Full list of author information is available at the end of the article

Introduction

Named after its colors, Chinese blue-and-white porcelain was one of the most popular trade products in Southeast Asia and beyond between the fifteenth and eighteenth centuries. The ware came mostly from Jingdezhen, the city of porcelain, and was manufactured in folk kilns while orders for the imperial court were fulfilled by official kilns [1]. For the latter, textual evidence indicates that the production organization was based on the division of labor with a strictly controlled and highly compartmentalized structure which contributed to maintaining a high level of constancy and quality [2, 3]. In contrast, and despite scant documentation, numerous archaeological findings from terrestrial and submerged sites point to a lot more variability among the ware for overseas markets produced in folk kilns, as for example color differences. The so-called blue-and-white porcelain is indeed not always blue and white, and the 'blue' decor could be gray or even black whereas the 'white' area could look grayish or beige. Besides, it can be noted that these atypical hues are not an issue for native speakers since the Chinese term for the products, *Qinghua,* meaning patterns with *qing* color, refers to a broad spectrum, ranging from green to black [4, 5]. In relation to this problem, color differences and glaze opacity could be repeatedly observed on the blue-and-white porcelain cargo of the Santa Cruz, one of the best-preserved shipwrecks in Southeast Asia [6], which raise questions about the origin of such notable features for ceramics in these contexts.

The Santa Cruz, a 25 m long junk, was found at a depth of 32 m about 10 km off the Zambales coast in the northern part of Luzon Island, the Philippines. Among its abundant cargo, there were more than 15,000 ceramics of various origins, including China, Vietnam, Siam, and Myanmar, reflecting a complex maritime trading network [7]. Chinese ware, mainly blue-and-white porcelain and celadon, accounted for as much as 86% of the ceramic discoveries and piles of the former were found in the bulkheads as loaded and almost intact, while pieces placed in the upper part of the boat were scattered around the wreck [8–12] (Fig. 1). Based on stylistic analysis, the blue-and-white porcelain was produced in

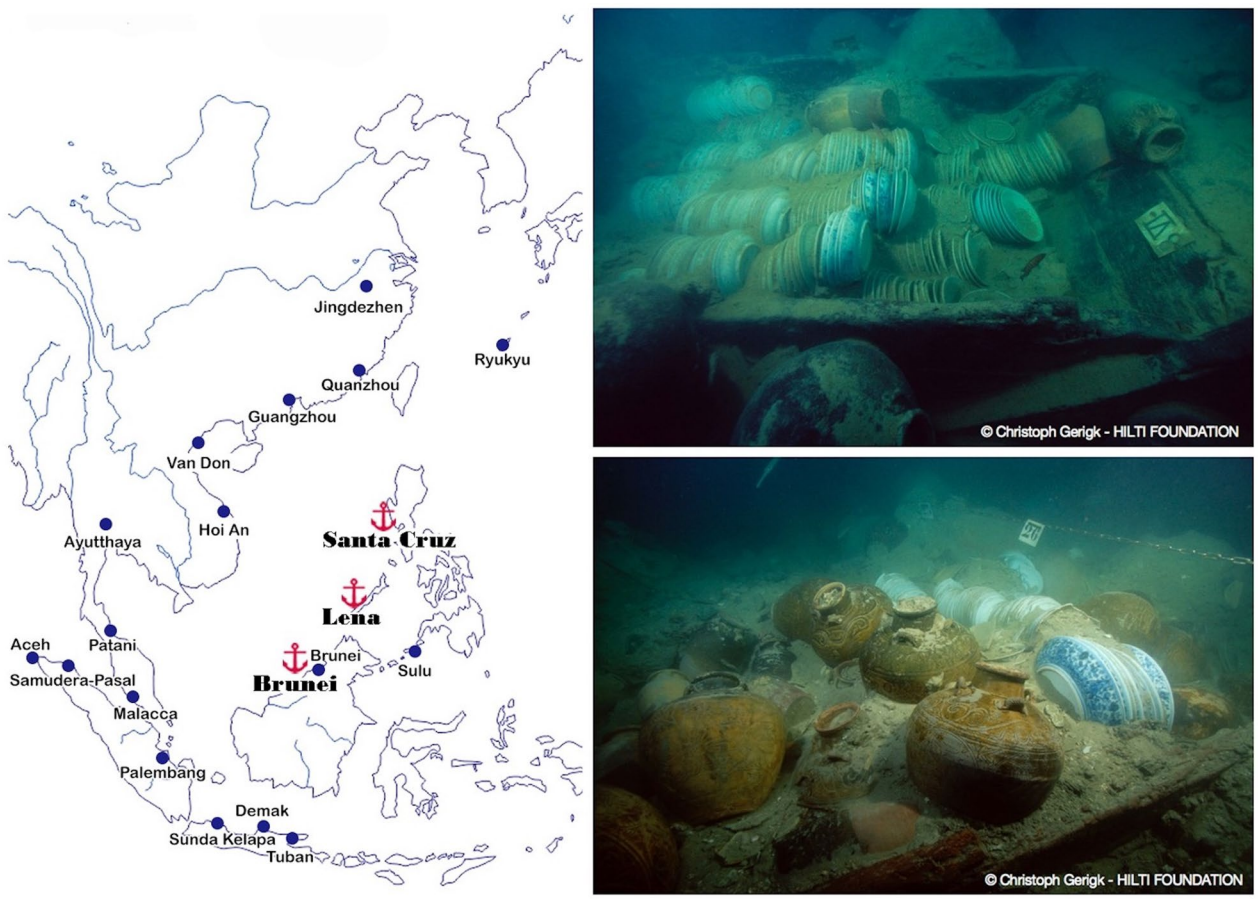

Fig. 1 Map of East and Southeast Asia with the location of the Santa Cruz Wreck (left) and images taken during the underwater excavation (right)

Jingdezhen during the Hongzhi period (1488–1505 CE) of the Ming Dynasty [13–16]. The prevalence of Chinese ware in the Santa Cruz, also observed for the Lena and Brunei wrecks, two other contemporary sunken junks found along the east side of the South China Sea, was considered exceptional since Chinese overseas activities declined between c. 1380–1580 due to the maritime ban from the Ming Court and Southeast Asian ceramics dominated the market [16–21]. Scholars have suggested that such high proportions of Chinese ware could be evidence of illicit trade [11] or a lessening of the ban [22].

Beyond these historical considerations, the Chinese blue-and-white porcelain in the Santa Cruz is of particular significance since records of representative pieces from the late fifteenth century are relatively few and indeed, mostly from shipwrecks. Moreover, as the ware loaded in a specific vessel was most likely from the same workshop, and hence considered relatively homogeneous, the occurrence of peculiar features makes it an interesting case to investigate factors and causes responsible for color variations and defects like glaze opacity.

Deterioration of glass and high-fired ceramic glazes: a brief overview

From a materials viewpoint, at first glance, the alteration of high-fired ceramic glazes (Ca-rich) and associated pigments in decorative patterns can be paralleled with the degradation (corrosion) of glass in general, and more specifically with colored, stained, and/or enameled glass, in particular the potash-lime-silica type commonly found in medieval stained-glass windows. The corrosion of glass is a multifaceted phenomenon primarily controlled by the chemical composition of the glass (e.g., soda-based glasses have much better durability than potash equivalents [23]) and the characteristics of the corrosion medium (composition, pH, temperature, etc.) as well as numerous other environmental, physical and biological factors [24–28] and references therein. The main process is best described by an ion-exchange mechanism where protonic species from the surrounding solution diffuse into the glass and replace network modifier cations which are leached out of the silicate matrix resulting in a cation-depleted silica-rich surface layer with lower density [29–31]. This basic mechanism is however associated with (or followed by) various complex reactions occurring in or at the surface of the modified layer, such as network depolymerization, interfacial dissolution-reprecipitation, secondary crystallizations and microcracks formation, which are essentially controlled by the pH of the solution as well as other microenvironmental parameters. Only recently has a clearer picture of the overall transformation process emerged owing to high-resolution analyses of ancient glass samples and model glass altered in natural or controlled conditions [26, 32–36]. Yet, the typology and micromorphology of the corrosion layer remain dependent on the complex interaction of many factors and hence, on the historical and/or archaeological context.

For example, medieval stained-glass windows and model analogs weathered in atmospheric conditions and different environments show an alteration crust with neoformed amorphous and/or crystalline phases, the latter usually composed of salts from the leached cations [33, 37–39]. Moreover, when crystallizations create a network of microcracks under the influence of cyclic climate variations, it can induce scaling at the surface of the glass and increase the alteration rate [40]. On sixteenth-to-twentieth-century enameled stained-glass windows, pronounced flaking of the glassy paint layer could be observed with a partial loss of the decorations and was correlated with an insufficient degree of vitrification of the enamel and/or a high concentration of K and low content of Ca and Pb [41]. The latter result is consistent with the known behavior of these elements, which can be easily leached out and contribute to the formation of the alteration layer while, for Ca and Pb, also increase the stability of the glass phase when present in higher concentrations [24, 42–44].

On the other hand, the weathering of glass in soils or underwater is characterized by a stratified alteration layer composed of iridescent laminated structures which can evolve in parallel, hemispherical or more complex patterns [35, 36, 45–50]. A comparative analysis of Roman glass buried in soil and seabed sediments has indeed shown that silica-rich laminations form in both environments, but in addition, an opaque and heterogeneous white crust of similar composition was only observed on submerged colorless glass, while in soils, the laminated structures contain Mn-rich (+Fe) phases, also found together with Ca and P inside cavities developed along microcracks, pointing to a probable external (soil) origin [48]. Likewise, the presence of Mn (and Fe) was identified in the laminated structures of archaeological fragments from stained-glass windows [51]. Manganese was associated with a darkening of the glass induced by the oxidation of Mn(II) ions and the precipitation of insoluble, black-colored Mn(IV)-rich phases. This reaction is of particular relevance here as darker, sometimes blackish, hues of the decorations on blue-and-white ceramics have been attributed to the oxidation of Mn (and Fe) associated with the Co-based pigment [52, 53].

Besides such differences, it seems that the two environments have a rather similar impact apart maybe from the faster corrosion kinetics in underwater contexts, possibly favored by the continuous replenishment of the contact solution, which often translates into thicker corrosion

crusts [48, 54]. Conversely, the underwater artefact-environment interface shows considerable variability, even at the scale of a wreck site [55], and the alteration rate can be significantly reduced in confined conditions [56] or when bio-colonization protects the glass surface [57].

Although observed in the alteration layer of tin glazes [58], the characteristic laminated structures have not been reported for Ca-rich glaze in high-fired ceramics, neither from land-based nor underwater archaeological contexts [59–62], and in general, this type of glaze is less prone to degradation. On excavated fragments of Jun porcelain (Song Dynasty), there was no alteration layer per se, and corrosion features were constrained to areas where wollastonite, a calcium silicate, had crystallized during firing and was partially 'dissolved' leaving dendritic or columnar pits and craters on the surface of the glaze [59]. Similar corrosion patterns, associated with a pronounced loss of transparency, were observed on the glazes of land-excavated Ru ware (Northern Song Dynasty) and underwater Longquan celadons (Dalian Island shipwreck, Yuan Dynasty) with a preferential dissolution of the Ca-rich component in the phase-separated glassy matrix within (or close to) the anorthite clusters [61, 62]. A shard from a black-glazed porcelain bowl (Southern Song Dynasty) buried in acidic soil and excavated at the Tushan kiln site (Chongqing, SW China) only showed a thin (~ 10 μm) amorphous silica-rich alteration layer and some thicker crust-like protrusions with heterogeneous micro-morphology and composition [60].

The corrosion resistance of high-fired ceramic glazes can be linked to their chemical composition. In comparison to potash-lime-silica glass, they contain less K and often less Ca (though still high), but critically, more Al (and Si) which contributes to increasing the stability of the glaze [63, 64]. Whenever such ware shows significant degradation, it appears that the corrosion patterns are connected to defects and heterogeneities in the glaze, notably the presence of wollastonite or anorthite crystals resulting from the devitrification during the firing process. Interestingly, these phases are absent in Vietnamese underglazed ceramics and celadons, and the ware, from both land and underwater contexts, is relatively well-preserved [65]. Moreover, the various shades of blue observed on blue-and-white sherds from the Chu Đâu-My Xa kiln site and Cù Lao Chàm shipwreck (but produced at the same kiln site) seem uncorrelated with the archaeological context and are more likely associated with the composition of the pigments used for the decorations [66]. However, the frosted appearance and loss of gloss on some sherds from the shipwreck indicate that chemical corrosion was active; an observation confirmed by the higher hydration state of the glaze surface detected with Raman microspectroscopy compared to a sherd from the kiln site [67]. Similar corrosion features have been observed on sherds from the blue-and-white cargo of several Portuguese shipwrecks while some sherds have kept their gloss, notably those from Kraak ware [68].

The deterioration of ancient glass and ceramic glazes has been analyzed with various spectroscopic, spectrometric and imaging techniques [54, 69–75]. Of particular interest are portable non-invasive techniques such as portable X-ray fluorescence (pXRF) and Raman spectroscopy which have been used for the in-situ analysis of glass, glazes and pigments [76–82]. In this paper, variations in the color of the blue decorations and the aspect of the glaze, notably the loss of transparency, have been researched by combining detailed visual observations with pXRF and another non-invasive and portable technique: fiber optics reflectance spectroscopy (FORS); the latter providing the raw data for quantitative colorimetric analysis. Results from scientific investigations were further compared with other studies and contextualized into the development of Jingdezhen at the turn of the sixteenth century.

Materials and methods

Blue-and-white porcelain

The selection of the blue-and-white ware was based on visual differences in color and aspect but constrained by both time and accessibility. Only a small part of the Santa Cruz cargo could be quickly surveyed in the storage room of the National Museum in Manila. Among the boxes which were open, all containing plates, one of the most common types in the assemblage, the color variability was impressive. For the purpose of this study, it was decided to focus on plates with atypical colors and peculiar features, and twelve plates were selected for analysis. In addition, a homogeneous set of objects with large flat surfaces was considered an advantage, particularly for the pXRF measurements. Originally, the porcelain plates were loaded in piles, mostly at the port side of the vessel, and distributed in bulkhead one, three, five, seven, and nine [8]. All of them are saucer-shaped and of similar size with a diameter of about 26 cm and a height of 4 cm, while their foot-ring diameter is about 13 cm. The interior blue decorations display casual-style motifs consisting of flowers, mainly chrysanthemums, and other plants as well as rocks, deer and pine trees (Fig. 2). All plates but one (SC-256) are also decorated on the exterior of the cavetto with floral patterns but dates or trademarks are absent at the bottom of the plates. Blue-and-white dishes with similar designs were found in other mid-Ming shipwrecks such as the Lena Shoal, the Brunei junk, Ko Samui and Laoniujiao N°1 [16, 18, 20, 83]. For example, the depiction of fallow deer, a symbol of Taoism, in association with the pine tree on SC-256 (a motif called

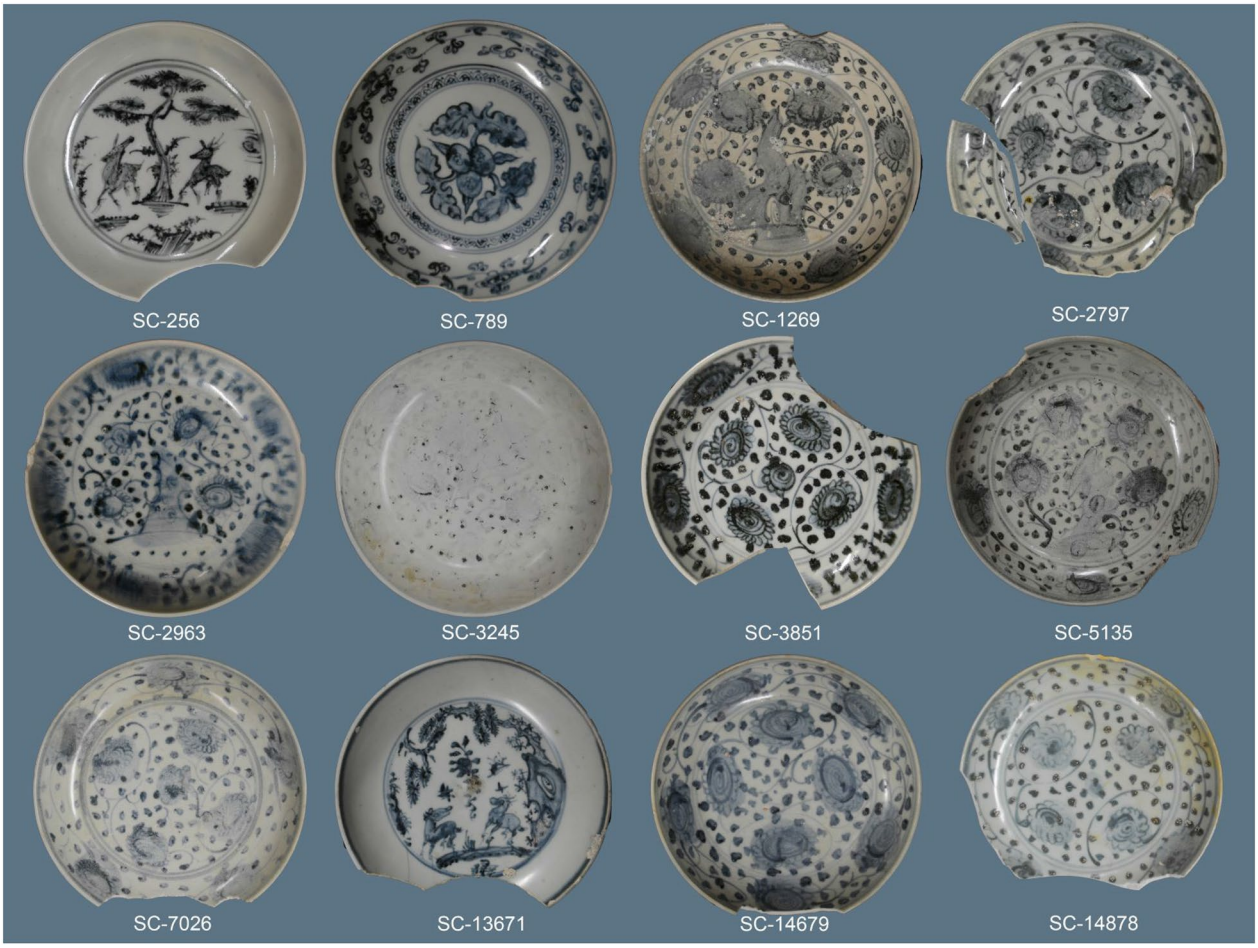

Fig. 2 Photographs of the twelve blue-and-white porcelain dishes from the Santa Cruz shipwreck analyzed in this study

'*Song Lu Zhang Chun*' in Chinese, meaning long life and wealth) is almost identical to the decoration on a dish (BRU376) from the Brunei junk [84].

The primary motifs are outlined and filled with light colors, whereas the small leaf patterns were drawn directly with thicker pigments favoring the formation of darker spots after firing. The glaze was applied on the whole dish, and for several of them, it appears slightly opaque rather than transparent; it was apparently scraped off the foot ring leading to a somewhat angular rim where the clay body is visible though irregularly. The glaze often shows defects such as crazing, pinholes and Y-shaped dewetting patterns (Fig. 3a, b). The latter two seem to be more developed on the bottom of the dishes which could be related to the different degree of finishing of the clay body compared to the decorated areas. While all dishes were cleaned and desalinated after the excavation, some still show marine calcareous encrustations (Fig. 3c). The main characteristics of the selected blue-and-white dishes are summarized in Table 1.

Methods

Portable X-ray fluorescence (pXRF)

Compositional data were obtained with a Thermo Niton XL3t GOLDD+handheld XRF spectrometer equipped with a silver anode tube and a large silicon drift detector (SDD) operating at a maximum voltage of 50 kV and current of 200 μA with a resolution better than 160 eV. Single pXRF measurements were carried out directly on the transparent glazed surface of the blue-decorated and 'white' areas with a standard spot diameter of about 6 mm, the built-in camera allowing precise positioning. Data were collected in both soil (blue and 'white') and mining (only 'white') modes with acquisition times set to 60 and 90 s, respectively. The two modes use different algorithms and proprietary calibrations for the conversion of counts into concentrations. From a practical viewpoint, the mining mode is better adapted for the

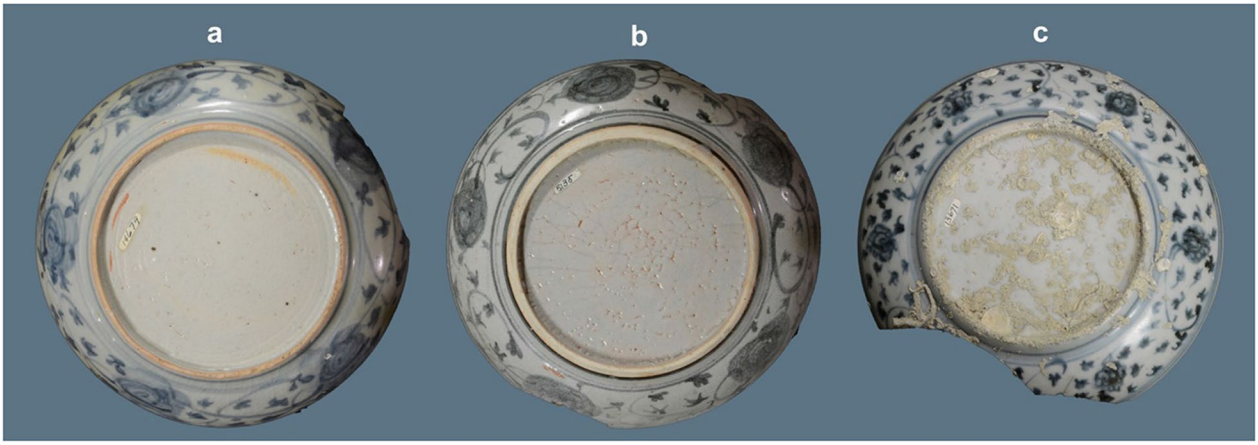

Fig. 3 Features on the bottom of three selected dishes. **a** Homogenous glaze with some defects (SC14679); **b** crazed glaze with pinholes and Y-shaped dewetting patterns (SC5135); **c** shell and worm-like encrustations (SC13671)

analysis of major and minor elements while the soil mode is optimized for elements present at trace levels; typically, above 0.5–1% for the former and in the tenths to thousands ppm range for the latter, depending on the element. Measurements on the blue decoration (glaze + blue pigment) and the 'white' were taken on the flat surface of the plate's interior while an additional 'white' was analyzed at the bottom. When the surface of the 'white' next to the blue on the interior was too small or inadequate, the 'white' was sometimes analyzed on the less decorated external side of the dishes. Additional information about the pXRF methodology and limitations of the technique can be found elsewhere [81] and references therein.

Table 1 Characteristics of the selected blue-and-white porcelain dishes

Reference	Grid location[a]	Motif	Glaze aspect and defects				Decoration color
			Aspect	Crazing	Load cracks	Dewetting	
SC-256	N22W5	Fallow deer and pine tree	Transparent, encrustations on foot-ring	o	o	+	Grayish green
SC-789	N19W7	Fruits and leaves	Transparent	o	+	++ (bottom)	Grayish blue
SC-1269	N19W8	Flora and rock	Slightly opaque with a frosted appearance, encrustations on the interior (+) and bottom (+++)	+++	+	++ (bottom)	Brownish gray
SC-2797	N27W5	Flora	Transparent, encrustations on foot-ring	++	++	++	Greenish gray
SC-2963	N29W5	Flora and rock	Transparent in the decorated areas, milky on the bottom	++	o	+	Blue
SC-3245	N29W5	Flora and rock	Opaque with a pronounced frosted appearance	++	?	++	Light gray
SC-3851	N30W7	Flora	Transparent in the decorated areas, milky on the bottom	o	+	++	Bluish gray
SC-5135	N25W10	Flora and rock	Semi-opaque	+++	+	+++	Gray
SC-7026	N31W7	Flora	Semi-opaque with a frosted appearance	+++	+	+	Light grayish blue
SC-13671	N36W7	Deer and pine tree	Transparent, numerous encrustations on the bottom	o	+	+	Grayish blue
SC-14679	N34W10	Flora	Slightly opaque with an apparent frosted appearance, milky on the bottom	+++	+	+	Blue
SC-14878	N34W5	Flora	Slightly opaque with a visible frosted appearance	o	o	+	Bluish gray

[a] Grid size is 1 square meter

Fiber optics reflectance spectroscopy (FORS)

Reflectance spectra were acquired with a portable FieldSpec®3 spectrometer (ASD Inc., Malvern Panalytical) in the 350 to 2500 nm spectral range with a resolution varying from 2 to 10 nm. Spectral data are internally re-sampled by the instrument to 1 nm intervals, and each collected spectrum corresponds to the average of thirty scans. Reflectance was measured with a high-intensity contact probe equipped with a halogen light source giving a spot diameter of about 10 mm and was calibrated against a white Spectralon® standard. Measurements were taken on the blue decorated areas and on the 'white'

Table 2 Elemental composition and absorptions in the visible spectral range of the selected blue-and-white porcelain dishes

Accession N°	Spot	Selected elements from pXRF analysis[a]												FORS analysis			
		Major (% oxides)		Minor and trace (ppm)										Spectral absorptions (nm)[b]			
		CaO	K_2O	Fe	Ti	Mn	Rb	Sr	Zr	Co	Cu	Th	Ni	Co (II)			H_2O
SC-256	Blue			2546	–	7265	408	87	46	1276	47	11	341	519 w	583 s	678 s	
	White	4.4	5.2	2104	116	340	412	95	45	–	28	8	–				
	Bottom	3.9	5.1	3833	84	495	403	71	58	–	28	17	71				
SC-789	Blue			4019	128	3035	385	99	44	279	37	10	244	517 m	582 s	673 m	
	White	6.1	4.0	3585	125	348	411	97	50	–	27	10	–				
	Bottom	5.5	4.0	3778	139	391	406	101	48	–	19	9	–				
SC-1269	Blue			2996	103	3038	385	82	57	442	54	11	206	521 vw	584 m	679 s	+++
	White	4.5	5.0	2553	251	326	392	87	53	–	33	11	83				
	Bottom	3.4	5.0	2351	187	254	395	62	63	–	28	12	57				
SC-2797	Blue			3375	115	1796	448	109	45	275	51	9	115	520 m	585 s	676 s	
	White	6.9	4.2	2697	116	295	408	136	40	–	32	–	67				
	Bottom	5.8	4.3	5350	228	371	475	122	56	–	37	15	77				
SC-2963	Blue			4678	–	3840	307	100	45	611	45	9	415	517 m	583 s	677 m	
	White	6.6	3.9	4591	–	440	318	95	53	–	37	10	107				
	Bottom	5.7	4.0	5640	95	464	326	72	59	–	26	14	83				
SC-3245	Blue			3484	–	2150	322	111	48	343	58	9	281	521 m	581 s	665 br	++
	White	5.4	4.2	2997	156	262	335	97	54	–	33	12	–				
	Bottom	5.5	4.3	2361	133	233	334	73	63	–	29	14	54				
SC-3851	Blue			3408	–	8910	333	94	50	1047	112	12	237	520 m	583 s	677 s	
	White	8.1	4.1	3194	148	602	331	112	49	–	52	12	87				
	Bottom	6.6	4.1	4437	229	439	361	78	62	–	32	16	82				
SC-5135	Blue			3376	285	2011	417	106	49	186	113	9	164	522 m	585 s	675 s	++
	White	5.6	4.2	3131	81	229	457	84	53	–	47	10	–				
	Bottom	5.0	4.7	3037	151	327	492	71	58	–	37	10	86				
SC-7026	Blue			2925	105	1305	573	88	39	133	48	8	218	519 m	583 s	670 s	++
	White	5.9	4.2	2835	202	240	601	92	48	–	24	–	–				
	Bottom	4.1	3.5	4373	266	310	669	42	57	–	19	18	–				
SC-13671	Blue			3884	133	3543	392	92	50	355	56	12	465	520 m	581 s	672 m	
	White	5.9	4.8	3061	191	428	394	91	52	–	49	10	111				
	Bottom	4.4	4.6	3794	117	398	414	66	55	–	29	13	64				
SC-14679	Blue			3416	103	2516	400	54	52	356	34	10	351	518 m	584 s	671 m	+
	White	5.9	4.3	2561	214	438	391	71	50	–	35	8	88				
	Bottom	4.9	4.5	3964	172	528	415	49	61	–	27	14	–				
SC-14878	Blue			4335	129	3169	539	84	45	166	71	21	701	522 m	586 s	655 br	
	White	5.9	4.6	3752	142	347	567	85	54	–	66	10	93				
	Bottom	4.9	4.1	5624	255	607	655	57	66	–	43	13	56				

[a] For major elements, values for Si and Al are considered qualitative and not reported

[b] Absorptions: vw: very weak, w: weak, m: medium, s: strong, br: broad

at the bottom because there was often not enough space for the measuring probe between the blue decor. Colorimetric data (XYZ) were extracted from the reflectance spectra and converted into the CIELAB chromatic color space and HEX color codes (http://www.easyrgb.com/en/) for analysis and visualization.

Results and discussion

Chemical composition and production kilns

In agreement with the historical context and stylistic analysis, elemental data obtained with pXRF on the transparent glaze confirm a Jingdezhen production for the blue-and-white plates based on the concentrations of some discriminative elements such as zirconium, thorium and titanium (Table 2). Values for these elements are close to the ones measured with pXRF and other techniques in previous studies despite the different time periods [81, 85–89]; such compositional similarities could correspond to a relative constancy in the procurement of raw materials and processing technologies from the middle to late-Ming period. However, variations in rubidium levels, i.e. the higher values reported in the present study, also found for the Guanyinge and other unspecified late-Ming kiln sites (Rb: 428 ± 78 ppm, [86]; Rb: 436 ± 84 ppm, [85]), compared to the lower averages measured on Jingdezhen blue-and-white ware from the Nan'ao One shipwreck in China (Rb: ~ 270 ppm, [86]) and sherds from the Philippines and Indonesia (315 ± 40 ppm, [81]) dated to the late-Ming and early-Qing periods, might reflect some intra-site variability among the numerous folk kilns in Jingdezhen.

As expected, the chemistry of the glaze analyzed in the 'white' area corresponds to an aluminosilicate glassy network containing calcium and potassium added as fluxing agents and network modifiers. The average amounts of Ca (CaO ~ 6.1 ± 0.9) and K (K_2O ~ 4.3 ± 0.4) are higher and lower, respectively, than those obtained with pXRF on sherds from the Xuande and Chenghua periods [89] but still in the range of Ca values known to have significantly varied (from a few to more than twelve percent CaO) throughout the Ming (and Qing) dynasty [68, 81, 87, 88, 90–93]. It should also be mentioned that because of the X-rays emission depth for Ca and K (about a few tenths of micrometers in this type of matrix) [94, 95], these two elements could be underestimated if the glaze is corroded on the surface. On the other hand, Ca seems not related to the degree of translucency of the glaze, making it challenging to identify the origin of the opacity which could be linked to the firing process and/or underwater weathering. For a few dishes, the low calcium levels, if associated with lower firing temperatures, could indirectly contribute to opacify the glaze through a silica matt effect. However, translucency has probably a different origin as the correlation with calcium levels is far from systematic.

Also noticeable are some significant differences in the composition of the glaze applied to the bottom, which shows lower calcium and higher iron levels in comparison to the glaze in the 'white' areas. Although there are exceptions to this trend (SC-3245 for Ca and Fe, SC-1269 and SC-5135 for Fe), it could suggest the usage of a modified recipe for the glaze applied to the bottom, which also implies a two-step glazing process. However, a systematic study on a much larger number of plates would be needed to exclude other explanations and confirm this hypothesis.

Blue decorations: pigment characteristics

The comparative analysis of pXRF data from the blue decorated and 'white' areas shows that the cobalt-based pigment contains high levels of manganese, low iron and significant amounts of nickel as well as traces of copper (Table 2) which points toward an Asian source [52]. After subtracting the manganese and iron contribution from the transparent glaze ('white' area), normalized percentages of Mn, Co and Fe are similar to the blue pigment analyzed on other export blue-and-white porcelain produced in Jingdezhen (Fig. 4, left). Although the heterogeneous distribution of the coloring elements and particles within the glaze, combined with the constraints on the probing depth, prevent a precise determination of the pigment's chemical composition, this elemental profile and the average Mn/Co ratio (7.1 ± 1.7) are consistent with results of previous studies [81, 87, 93, 96, 97] and confirm the use of Mn-rich asbolane ores in folk kilns during the Hongzhi period of the Ming dynasty.

Spectral profiles obtained with FORS on the blue decorated areas (Fig. 4, right) show the characteristic absorptions of Co(II) in tetrahedral coordination with the triplet located around 520, 583 and 672 nm [81, 98]. For some plates, darker colors translate in an overall lower reflectance in the visible, but the cobalt absorptions with variable relative intensities are always present (Table 2). The gray-greenish or blackish hue of the decoration is most likely correlated with the manganese and iron in the pigment, combined with redox firing and cooling conditions favoring the crystallization of Mn and Fe-rich oxide phases [52, 53, 93].

Similar dark colors were also observed on blue-and-white sherds from the late fifteenth to the early sixteenth centuries by Wang et al. [99] and Qu et al. [100]. More specifically, these colors have been connected with the crystallization of Mn(Fe)-rich spinels [101, 102] in dark spots which parallel the 'iron spots' observed on Yuan and early-Ming blue-and-white

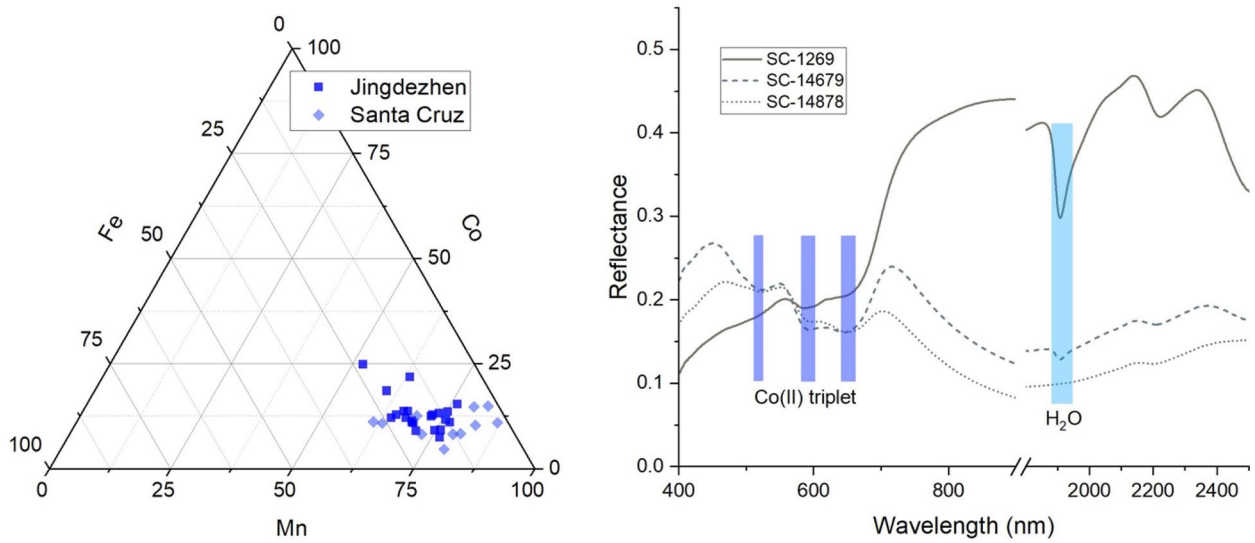

Fig. 4 Ternary plot visualizing the blue pigment composition based on the relative proportions of Co, Mn and Fe; Santa Cruz data compared to a set of Jingdezhen blue-and-white from [87] (left). FORS spectra with the main absorptions of Co(II) in the visible and water in the near-infrared obtained on decorated areas for three plates from the analyzed set (right)

when imported Fe-rich Co-pigment was in use [53]; in fifteenth century Vietnamese blue-and-white, a dark-greenish blue tint was even obtained intentionally by adding iron [103]. In our FORS spectra, although the presence of Mn-rich phases might be associated with weak absorptions (only visible on 2nd derivative spectra) at ~ 420 nm Mn(II) and ~ 490 nm Mn(III), the correlation is not well-established despite a thorough study of the spectral profiles. The analysis is complicated by the probable contribution of various Fe(III) absorptions to the overall spectral profile below 500 nm [104, 105]. Further research is definitely needed, notably on reference materials, to make more solid interpretations using the potential of FORS.

Finally, in the near-infrared spectral range, some plates show an asymmetrical absorption of variable intensity around 1910 nm corresponding to the combination band ($\nu_{OH}+\delta_{HOH}$) of water which could be adsorbed in the glaze and/or in the body. The presence of water might be due to weathering and/or indirectly reflect a residual porosity in the body resulting from lower firing temperatures. Depending on its location, water could be a contributing factor to the opacity, a possibility that would require additional specific analysis.

Color, technology and weathering

Visual observations

The pictures in Fig. 2 clearly show variations and alterations in the appearance of both the glaze and the blue decorations. As described earlier, surface corrosion and abrasion on ceramic ware recovered from shipwrecks is not uncommon [62, 68] and the weathering induced by the immersion in seawater for hundreds of years has certainly contributed to some of the features observed here. It does not explain however why several dishes in the same environment still look almost pristine. Moreover, the striking differences between dishes excavated from the same grid (e.g., SC-2963 and SC-3245) indicate that location in the wreck is not a prime factor and point to other causes.

The glaze of most dishes is rather transparent but for a few it tends to be slightly opaque with sometimes a milky and/or frosted appearance. This translucency affects the visibility of the decoration underneath which shows significant differences in the hue and brightness of the Co-based pigment. The blue areas often look dull with the naked eye and have a greenish or grayish tint. Intriguingly, this color shift was also frequently observed on blue-and-white ware from contemporaneous shipwrecks such as the Lena and Brunei junks [16, 20, 84]. Occasionally, a brownish material can be observed on top of the dark blue areas, often in association with whitish spots marked by a network of needle-like crystals (Fig. 5) similar to the clusters of anorthite or wollastonite identified in the corroded areas on other types of high-fired glazed ceramics mentioned earlier [59, 61, 62]. Here, they are probably composed of anorthite ($CaAl_2Si_2O_8$), which is the main crystalline phase found in traditional glazes [106] as well as in modern Al-rich glaze formulations when firing cycles include longer soaking times favoring devitrification [107]. Although the presence of

anorthite in the glaze of blue-and-white porcelain has been reported in numerous studies, the crystals are usually located at the body-glaze interface in close association with the cobalt pigment [99, 100, 108–111]. They are rarely found throughout the whole thickness of the glaze or near the surface as observed for dish SC-14878.

Interestingly, a sherd from the Guthe collection (GU09, Fischer and Hsieh [81]) might provide some clues about the features observed on dish SC-14878 as it displays similar surface patterns (Fig. 6, left). Scanning electron micrographs in backscattered electron mode show indeed anorthite (confirmed with energy dispersive spectroscopy analysis) crystals at the surface of the glaze with a partial dissolution of the interstitial glass phase (Fig. 6, center) while the cross-section reveals insightful details about the glaze microstructure and anorthite distribution (Fig. 6, right). It is generally assumed that anorthite crystallizes at the glaze-body interface because of a change in the glaze composition near the interface resulting from the partial melting of the body and subsequent diffusion of aluminum [112]. Here though, anorthite crystals are not only visible at the interface but within the entire thickness of the glaze. Moreover, the pigmented layer with Co-rich particles embedded in the network of anorthite, usually found close to the body, is located near the surface, indicating that it was lifted in the molten glaze by further bottom-up crystallization and growth of anorthite which might be favored by longer soaking times at high temperature. Likewise, the formation, growth and migration of bubbles can have a similar effect (e.g., Pinto et al. [111], Fig. 7d). This mechanism not only explains the anorthite spots but also creates a (sub)surface heterogeneous microstructure particularly sensitive to dissolution and oxidation reactions that can affect the residual glassy matrix and elements originally associated with the pigment such as Mn, Fe and Ni, and possibly produce color changes. Less specifically, if the anorthite crystallization in the glaze is extensive, it can reduce the transparency by scattering the light and contribute to the surface mattness [107] which most likely explains the appearance of dishes SC-3245 and SC-7026.

Another explanation for the presence of the Co-pigment + anorthite near the surface could be the two-layers glaze technology described for sherds of

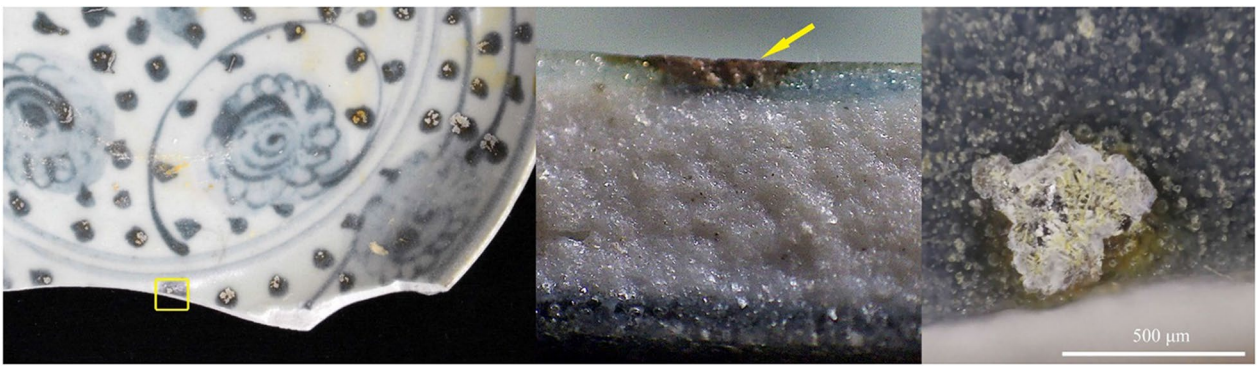

Fig. 5 Details of a dark blue decoration on the broken edge of dish SC-14878 showing the change to a brownish color (arrow) and the network of whitish minerals (right, top view)

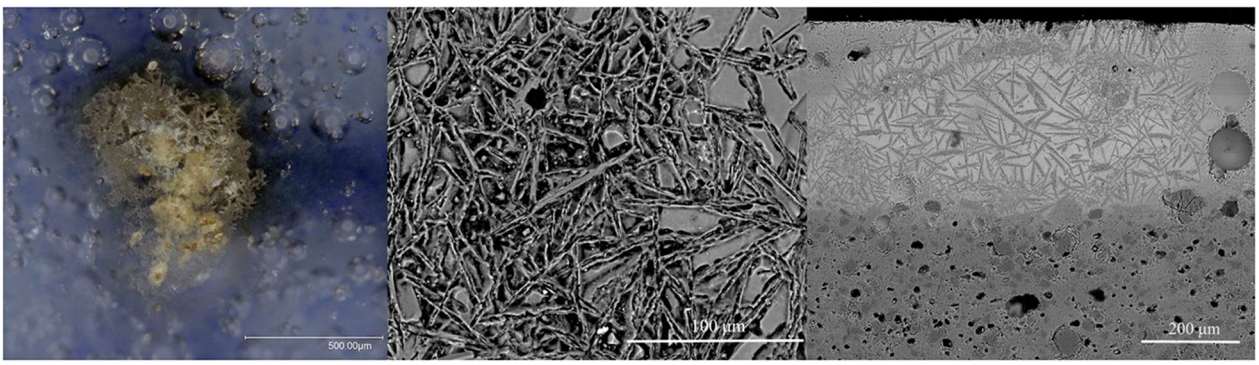

Fig. 6 Brownish spot on the sherd GU09 observed with a digital microscope (left) and a scanning electron microscope (NanoSEM^{TM}230, FEI): same surface (center) and corresponding cross-section (right)

blue-and-white export ceramics from China as well as Vietnam [68, 113–116]. Contrary to the traditional underglaze blue-and-white, in the two-layers technology the body was glazed and fired twice with the blue decoration applied in between after the first firing. The presence of two glaze layers has been recognized through observations and analyses on cross-sections with optical (+digital) microscopy and scanning electron microscopy coupled with energy dispersive X-ray spectroscopy for elemental analysis (SEM–EDS). The two layers appear to have a different composition with notably higher Ca in the upper layer which imparts both a better chemical stability to the glaze and a lower melting point avoiding re-melting of the first glaze layer during the second firing. However, SEM images were often taken at too low magnification to clearly visualize the two layers and the spatial organization of the different phases in the colored glaze [114], or not shown at all while EDS spectra are plenty [68]. Furthermore, elemental data were preferentially collected in the colored glaze, where Ca-rich crystalline phases can potentially affect the Ca value (requiring precise analysis location frequently not indicated), and sometimes compared to only one measurement in the colorless glaze. In fact, Ca concentrations should be systematically measured in the inner and outer parts of the colorless glaze as well in order to confirm the existence of two glaze layers, as exemplified by Zhang's EDS analysis, with two sherds showing such robust compositional evidence (114, Table 2, samples 1 and 10). Although beyond the research presented here, these experimental limitations and the importance of the topic certainly warrant further investigations. Finally, the sherds are all late-Ming productions, either from Fujian kilns [114, 115] or unspecified kiln sites [68], and only one is purportedly attributed to Jingdezhen ([113], sample N2), calling into question whether the technology was ever implemented in Jingdezhen, and all the more so during the mid-Ming period, making for now this alternative explanation unlikely.

All these observations and hypothesis suggest a critical role of pre-existing characteristics determined by the original quality and aspect of the ware in relation to manufacturing technology and raw materials composition, particularly of the Co-based pigment. In an attempt to explore further causal links and key parameters, color variations were investigated more systematically through a quantitative approach based on colorimetry.

Color analysis

Color variations between the different plates were analyzed after converting the XYZ colorimetric data obtained with FORS into the CIELAB color space (Table 3). Also referred to as L*a*b*, in this representation, L* corresponds to the brightness while a* indicates the red and green hues for positive and negative values, respectively, and for b* similarly the yellow and blue, with intensifying blue as negative values increase for the latter [117]. In Fig. 7, coordinates b* are plotted in function of a* using corresponding HEX color codes for the symbols. Data include the chromaticity values of the Santa Cruz dishes (SC) and for comparison, those of some mid to late Ming blue-and-white porcelain excavated from the Maojiawan archaeological site, Beijing, but produced in Jingdezhen (TZ, Pinto et al. [111]). Some modern cobalt aluminate blue pigments synthesized by various methods were also added as reference (CB) [118–120].

For most Santa Cruz dishes, color parameters are characterized by negative a* and negative (or slightly positive) b* values not exceeding −15 which is consistent with the overall weak blue tint. These chromatic values are similar to the ones of sherds dated to the mid-fifteenth to the early sixteenth centuries analyzed and classified by Pinto et al. [111] in groups B and C ($-16 < b^* < 4$; $-4.2 < a^* < -3$). On the other hand, in the same study, sherds from the late Ming period (group A, TZ08-11) have a more pronounced blue tint, as shown by the higher b* negative values ($b^* \sim -23$). But these levels are still far from b* values obtained for modern Co–Al pigments synthesized through wet-chemistry processes [119, 120] or with oxide powder precursors [118] and calcinated at various temperatures (Table 4). The difference between CB-1a and CB-1b exemplifies the well-known role of the firing temperature on the blue color of cobalt

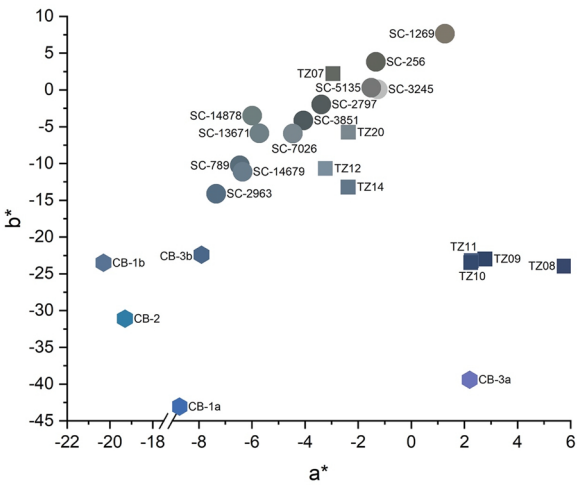

Fig. 7 2D scatterplot of chromaticity values a* and b* with corresponding CIELAB colors. Reported data include measurements on the dishes from the Santa Cruz (SC), mid to late Ming blue-and-white sherds (TZ, Pinto et al. [111]) and various modern Co–Al blue pigments (CB). See text for additional information and refs

Table 3 Colorimetric data from FORS

Reference	XYZ data (1964 10°)			CIELAB data			HEX
	X	Y	Z	L*	a*	b*	
SC-256	13.55	12.39	3.88	41.83	−1.33	3.81	61645C
SC-789	14.47	14.04	6.56	44.29	−6.45	−10.26	596D7A
SC-1269	20.26	17.91	5.08	49.39	1.65	7.85	7A7468
SC-2797	10.64	10.00	3.75	37.84	−3.39	−1.97	525B5C
SC-2963	14.58	14.29	7.35	44.65	−7.34	−14.11	566E81
SC-3245	56.19	51.04	17.94	76.70	−1.26	0.09	BBBEBD
SC-3851	10.17	9.66	3.88	37.22	−4.06	−4.15	4F5A5E
SC-5135	20.30	18.52	6.47	50.12	−1.30	0.29	757,877
SC-7026	24.32	22.87	9.28	54.94	−4.46	−5.93	79878E
SC-13671	21.36	20.39	8.31	52.27	−5.72	−5.89	6F8187
SC-14679	19.55	18.81	8.74	50.46	−6.35	−11.13	687C8B
SC-14878	20.53	19.66	7.57	51.45	−5.99	−3.51	6E7F80

aluminates [121, 122]. Interestingly, Llusar et al. [118] show how the mixing of the Co–Al pigment (CB-3a) with a porcelainized glaze results in a less intense blue tint which could be due to some dissolution of the Co–Al spinel in the molten glaze in addition to the lower cobalt concentration effect.

However, a major difference is that the modern Co–Al pigments are 'pure' and do not contain Mn and/or Fe, which conversely could confirm the role of these elements in the development of darker grey-black or greenish hues for the blue decoration as argued by several authors, even if in the process the respective contribution of Mn and Fe-rich phases is still debated [99, 111]. The connection with color changes is not straightforward anyway because there is no direct correlation between decreasing b* values and higher manganese and/or iron levels. Multiple variables might be involved such as pigment particles' composition, structure, density and size as well as the use of mixtures [110, 111], not to mention the upstream influence of cobalt ore processing and firing conditions.

Table 4 Color parameter b* and calcination conditions for modern Co–Al blue pigments ($CoAl_2O_4$ spinel) prepared by various methods

Authors	Reference (Fig. 7)	b*	Temperature (°C)	Soaking time (h)
Tang et al. [120]	CB-1a	−43.1	1250	1
	CB-1b	−22.4	1150	1
Peymannia et al. [119]	CB-2	−31.1	1100	1
Llusar et al. [118]	CB-3a	−39.4	1400	3
	CB-3b[a]	−22.4	1185	1

[a] CB-3a pigment mixed with porcelainized glaze (1:5) and enameled on biscuit

From a historical viewpoint, it is worth mentioning that blue-and-white porcelain produced during the Hongzhi period is often described as unremarkable by art historians because associated with minor technological and stylistic innovations even if the porcelain ware equaled the outstanding achievements of the preceding Chenghua period (1464–87 CE). The latter though ended with unsustainable production costs for the imperial factory and thus, to avoid further straining the court's finances, the Hongzhi emperor decided to almost halt the operation of official kilns entirely during his reign [123]. Moreover, the Chenghua period marked the transition from imported cobalt pigments to local asbolane ores, which were seemingly easier to grind resulting in a finer pigment but fired to a greyish shade of blue [124]. This color particularity was also noted by Valenstein [125] for blue-and-white ware produced during the following Zhengde period. Therefore, it can be argued that the apparent 'predominance' of greyish-blue hues during the Hongzhi and Zhengde periods was primarily due to a trial-and-error experimental approach in relation to the procurement and processing of cobalt-rich pigments from the newly exploited domestic sources. This could be supported by a mid-Ming blue-and-white porcelain bowl found at the Zhushan official kiln site (Fig. 8). The distinct colors of the numbered decorative motifs show that this ware was used to evaluate various cobalt-based pigments, possibly from different sources and refining methods and/or applied in mixtures.

Additionally, the ware attributes from folk kilns fluctuated much more compared to official kiln productions, most likely because of looser quality controls inherent to the large volumes manufactured for overseas markets and more variability in the pigment raw

Fig. 8 Blue-and-white porcelain bowl from the Ming dynasty apparently used for the evaluation of different types or formulations of Co-based pigments (Museum of Official Kiln, Jingdezhen)

materials. In this context, blue color standardization might not have been a primary concern for the traders on the Santa Cruz, knowing for example that Southeast Asian customers had used greyish ware from Vietnam and Siam for decades [126]. Although less frequent, quality differences also occurred later when trade expanded further if one refers to the notes by Italian Jesuit Matteo Ricci (1552–1610 CE) mentioning that skilled craftsmen did not seek perfection since buyers were satisfied with less finished goods [127].

Conclusion

This research has investigated variations in the appearance and color of blue-and-white porcelain recovered from the late fifteenth-century Santa Cruz shipwreck, with a particular focus on the aspect of the glaze and the peculiar hues of the blue decorations. In agreement with stylistic studies and historical data, compositional analysis has shown that the ware was produced in Jingdezhen, and the pigment for the 'blue' decorations was processed from Co-Mn-Ni-rich domestic asbolane ores.

Based on visual observations and microtextural comparisons, the origin of the opacity of the glaze was linked to the extensive crystallization of anorthite and its distribution in the glaze layer. In the blue-decorated areas of some plates, the anorthite laths associated with pigment particles reached the surface of the glaze, probably during prolonged soaking times, and subsequently formed white-brownish spots enhanced by weathering-induced dissolution and oxidation reactions. Chromaticity analysis has confirmed the visual perception of a grey-greenish, occasionally even blackish color of the 'blue' decorations, which contrasts with the brighter and lighter, sometimes deeper blues characteristic of the Yuan, early Ming and, to a lesser extent, late Ming periods.

While atypical hues and attributes variability have been known throughout the production history of Chinese blue-and-white porcelain, it is suggested here that their widespread occurrence in folk kiln ware of the Hongzhi and Zhengde periods reflects a phase of experimentation prompted by the transition from imported to domestic cobalt pigments. The blue-and-white cargo of the Santa Cruz and other junks of the same period thus indirectly reveal some of the changes that happened in the capital of porcelain at the turn of the sixteenth century when production in folk kilns ramped up significantly to satisfy the demand from abroad. It also shows that the line of causality extends well beyond the sunken history of the ware, back to its manufacture and, more specifically,

to the characteristics and processing of the pigment raw materials. On the other hand, it raises essential questions about the difficulties faced by potters and other craftsmen, from technological challenges and organizational constraints to the intricate concept of quality, and hence value, especially when comparing production in folk and official kilns, questions of which our limited understanding calls for further research.

Acknowledgements
We thank Dr. Mary Jane Louise A. Bolunia, National Museum of the Philippines, for granting access to the Santa Cruz collection. We also thank the late Ms. Lingyi Zeng, who introduced museums in Jingdezhen to one of the authors.

Author contributions
EH was responsible for funding acquisition, conceptualization, data collection, investigation and writing-review. CF was responsible for data collection and interpretation, investigation and writing-review. BO provided the archaeological contexts of the Santa Cruz Shipwreck. All authors read and approved the final manuscript.

Funding
This study was supported by UCLA Harry and Yvonne Lenart Graduate Travel Fellowships and the National Science and Technology Council Research Fund of Taiwan (Grant No. MOST110-2410-H-007-003-MY3).

Availability of data and materials
All data generated or analyzed during this study are included in this published article.

Declarations

Competing interests
The authors declare that they have no competing interests.

Author details
[1]Institute of Anthropology, Research Center for Underwater Archaeology and Heritage, National Tsing Hua University, No. 101, 2nd Sec. Guangfu Rd., Hsinchu City 300, Taiwan. [2]5378 Village Green, Los Angeles, CA 90016, USA. [3]Maritime and Underwater Cultural Heritage Division, National Museum of the Philippines, Padre Burgos Ave, Ermita, 1000 Manila, Metro Manila, The Philippines.

Received: 21 November 2022 Accepted: 3 May 2023
Published online: 15 May 2023

References

1. Finlay R. The pilgrim art: culture of porcelain in world history. Berkeley: University of California Press; 2010.
2. Julien S. Histoire et fabrication de la porcelaine chinoise. Paris: Mallet-Bachelier; 1856.
3. Gerritsen A. The city of blue and white: chinese porcelain and the early modern world. Cambridge: Cambridge University Press; 2020.
4. Tao J, Wong J. The confounding mandarin colour term 'Qīng': Green, blue, black or all of the above and more? In: Sadow L, Peeters B, Mullan K, editors. Studies in ethnopragmatics, cultural semantics, and intercultural communication. Singapore: Springer; 2020. p. 95–116.
5. Lam W-YN. A study of the color word "qing" and its combination: The University of Hong Kong; 2012.
6. Goddio F, Fabre D, Coignard M-A, editors. On-going archaeological researches on shipwrecked junks in the Philippines. Proceedings of the 2014 Asia-Pacific Regional Conference on Underwater Cultural Heritage; 2014; Honolulu.
7. Kimura J. The Packing and Loading of Ceramics Seen from Shipwrecks. In: Sasaki T, editor. The Archaeology of Medieval and Early Modern Ceramics. 8. Tokyo: Yuzankaku; 2018. p. 103–28.
8. Orillaneda BC. The Santa Cruz, Zambales Shipwreck Ceramics: Understanding Southeast Asian Ceramic Trade during the Late 15th Century C.E.: National University of the Philippines; 2008.
9. Orillaneda BC. The Santa Cruz shipwreck excavation: a reflection on the practice of underwater archaeology in Philippine. In: Tan H, editor. Marine archaeology in Southeast Asia: innovation and adaptation. Singapore: Asian Civilisation Museum; 2012. p. 87–102.
10. Orillaneda BC. Insights into Southeast Asian maritime trade during the 15th Century: Asian ceramics from the Santa Cruz shipwreck in the Philippines. In: Tripati S, editor. Maritime contacts of the past: deciphering connections amongst communities. Delhi: Kaveri Books; 2015. p. 300–26.
11. Orillaneda BC. Of Ships and Shipping: The Maritime Archaeology of Fifteenth Century CE Southeast Asia. Early Navigation in the Asia-Pacific Region: Springer; 2016. p. 29–57.
12. Orillaneda BC. Maritime trade in the philippines during the 15th century CE. Moussons. 2016;27:83–100.
13. Gotuaco L, Tan RC, Diem AI. Chinese and Vietnamese blue and white wares found in the Philippines. Makati City, Philippines: Bookmark; 1997.
14. Crick M. The Santa Cruz Wreck 2001: Preliminary archaeological report and ceramic cargo study. Manila: Far Eastern Foundation for Nautical Archaeology; 2001.
15. Tan RC. Chinese Blue and White Ware of the 14th to 15th Centuries: A Philippine Perspective. In: Jianxi Provincial Museum and The Art Museum at the Chinese University of Hongkong, editor. Yuan and Ming Blue and White Ware From Jiangxi. Hong Kong: The Art Museum at the Chinese University of Hongkong; 2002. p. 30–58.
16. Pirazzoli-t'Serstevens M. The Brunei shipwreck: A witness to the international trade in the China Sea around 1500. The Silk Road. 2011;9:5–17.
17. Brown RM. History of shipwreck excavation in Southeast Asia. In: Ward J, Kotitsa Z, D'Angelo A, editors. The Belitung wreck: Sunken treasures from Tang China. New Zeeland: Seabed Explorations; 2004. p. 40–55.
18. Brown RM. The Ming gap and shipwreck ceramics in Southeast Asia: Towards a chronology of Thai trade ware: Siam Society; 2009.
19. Goddio F, Pierson S, Crick M, editors. Sunken treasure: fifteenth century Chinese Cermaics from the Lena cargo. London: Periplus; 2000.
20. Goddio F, Crick M, Lam P, Pierson S, Scott R. Lost at Sea: the strange route of the Lena Shoal junk. London: Periplus; 2002.
21. Karim bin Pengiran Haji Osman. The Brunei Shipwreck: A Catalogue of Some Selected Artefacts and Brunei's Ancient Trade Products. Brunei: Ministry of Culture, Youth and Sport; 2015.
22. Tai YS, Daly P, Mckinnon EE, Parnell A, Feener RM, Majewski J, et al. The impact of Ming and Qing dynasty maritime bans on trade ceramics recovered from coastal settlements in northern Sumatra, Indonesia. Archaeol Res Asia. 2020;21:1–18.
23. Jackson C, Greenfield D, Howie L. An assessment of compositional and morphological changes in model archaeological glasses in an acid burial matrix. Archaeometry. 2012;54(3):489–507.
24. Paul A. Chemistry of glasses. London: Springer; 1989.
25. Melcher M, Schreiner M. Glass degradation by liquids and atmospheric agents. In: Janssens K, editor. Modern methods for analysing archaeological and historical glass. London: Wiley; 2013. p. 609–51.
26. Palomar T, Chabas A, Bastidas DM, de la Fuente D, Verney-Carron A. Effect of marine aerosols on the alteration of silicate glasses. J Noncryst Solids. 2017;471:328–37.
27. Majérus O, Lehuédé P, Biron I, Alloteau F, Narayanasamy S, Caurant D. Glass alteration in atmospheric conditions: crossing perspectives from cultural heritage, glass industry, and nuclear waste management. NPJ Mater Degradat. 2020;4(1):27.
28. Macedo MF, Vilarigues MG, Coutinho ML. Biodeterioration of glass-based historical building materials: an overview of the heritage literature from the 21st century. Appl Sci. 2021;11(20):9552.
29. Doremus RH. Diffusion-controlled reaction of water with glass. J Noncryst Solids. 1983;55(1):143–7.

30. Bunker B. Molecular mechanisms for corrosion of silica and silicate glasses. J Noncryst Solids. 1994;179:300–8.
31. Sterpenich J, Libourel G. Water diffusion in silicate glasses under natural weathering conditions: evidence from buried medieval stained glasses. J Noncryst Solids. 2006;352(50):5446–51.
32. Tournié A, Ricciardi P, Colomban P. Glass corrosion mechanisms: a multiscale analysis. Solid State Ionics. 2008;179(38):2142–54.
33. Lombardo T, Gentaz L, Verney-Carron A, Chabas A, Loisel C, Neff D, et al. Characterisation of complex alteration layers in medieval glasses. Corros Sci. 2013;72:10–9.
34. Hellmann R, Cotte S, Cadel E, Malladi S, Karlsson LS, Lozano-Perez S, et al. Nanometre-scale evidence for interfacial dissolution—reprecipitation control of silicate glass corrosion. Nat Mater. 2015;14(3):307–11.
35. Schalm O, Anaf W. Laminated altered layers in historical glass: density variations of silica nanoparticle random packings as explanation for the observed lamellae. J Noncryst Solids. 2016;442:1–16.
36. Schalm O, Nuyts G, Janssens K. Some critical observations about the degradation of glass: the formation of lamellae explained. J Noncryst Solids. 2021;569:120984.
37. Melcher M, Schreiner M. Statistical evaluation of potash-lime-silica glass weathering. Anal Bioanal Chem. 2004;379:628–39.
38. Melcher M, Schreiner M. Evaluation procedure for leaching studies on naturally weathered potash-lime-silica glasses with medieval composition by scanning electron microscopy. J Noncryst Solids. 2005;351(14–15):1210–25.
39. Melcher M, Schreiner M. Leaching studies on naturally weathered potash-lime–silica glasses. J Noncryst Solids. 2006;352(5):368–79.
40. Gentaz L, Lombardo T, Chabas A, Loisel C, Neff D, Verney-Carron A. Role of secondary phases in the scaling of stained glass windows exposed to rain. Corros Sci. 2016;109:206–16.
41. Schalm O, Van der Linden V, Frederickx P, Luyten S, Van der Snickt G, Caen J, et al. Enamels in stained glass windows: preparation, chemical composition, microstructure and causes of deterioration. Spectrochim Acta, Part B. 2009;64(8):812–20.
42. Colomban P, Liem NQ, Sagon G, Tinh HX, Hoành TB. Microstructure, composition and processing of 15th century Vietnamese porcelains and celadons. J Cult Herit. 2003;4(3):187–97.
43. Pradell T, Molina G, Murcia S, Ibáñez R, Liu C, Molera J, et al. Materials, techniques, and conservation of historic stained glass "Grisailles." Int J Appl Glas Sci. 2016;7(1):41–58.
44. Arévalo R, Mosa J, Aparicio M, Palomar T. The stability of the Ravenscroft's glass. Influence of the composition and the environment. Journal of Non-Crystalline Solids. 2021;565:120854.
45. Brill RH. Ancient glass. Sci Am. 1963;209(5):120–31.
46. Cox GA, Ford BA. The corrosion of glass on the sea bed. J Mater Sci. 1989;24:3146–53.
47. Cox GA, Ford BA. The long-term corrosion of glass by ground-water. J Mater Sci. 1993;28(20):5637–47.
48. Silvestri A, Molin G, Salviulo G. Archaeological glass alteration products in marine and land-based environments: morphological, chemical and microtextural characterization. J Noncryst Solids. 2005;351(16):1338–49.
49. Doménech-Carbó M-T, Doménech-Carbó A, Osete-Cortina L, Saurí-Peris M-C. A study on corrosion processes of archaeological glass from the Valencian region (Spain) and its consolidation treatment. Microchim Acta. 2006;154:123–42.
50. Gulmini M, Pace M, Ivaldi G, Ponzi MN, Mirti P. Morphological and chemical characterization of weathering products on buried Sasanian glass from central Iraq. J Noncryst Solids. 2009;355(31–33):1613–21.
51. Schalm O, Proost K, De Vis K, Cagno S, Janssens K, Mees F, et al. Manganese staining of archaeological glass: the characterization of Mn-rich inclusions in leached layers and a hypothesis of its formation. Archaeometry. 2011;53(1):103–22.
52. Colomban P, Kırmızı B, Simsek FG. Cobalt and associated impurities in blue (and green) glass, glaze and enamel: relationships between raw materials, processing, composition, phases and international trade. Minerals. 2021;11(6):633.
53. Wang W, Sciau P, Zhu J, Jiang J, Wen R, Brunet M. Microstructure analysis of "iron spots" on Qinghua porcelain from Jingdezhen imperial kiln. J Eur Ceram Soc. 2023;43(2):708–17.
54. Barbana F, Bertoncello R, Milanese L, Sada C. Alteration and corrosion phenomena in Roman submerged glass fragments. J Noncryst Solids. 2004;337(2):136–41.
55. Florian MLE. The underwater environment. In: Pearson C, editor. Conservation of marine archaeological objects. Oxford: Butterworth-Heinemann; 1987. p. 1–20.
56. Verney-Carron A, Gin S, Libourel G. A fractured roman glass block altered for 1800 years in seawater: analogy with nuclear waste glass in a deep geological repository. Geochim Cosmochim Acta. 2008;72(22):5372–85.
57. Palomar T. Characterization of the alteration processes of historical glasses on the seabed. Mater Chem Phys. 2018;214:391–401.
58. Doménech-Carbó MT, Mai-Cerovaz C, Doménech-Carbó A. Application of focused ion beam-field emission scanning electron microscopy-X-ray microanalysis in the study of the surface alterations of archaeological tin-glazed ceramics. Ceram Int. 2022;48(10):14067–75.
59. Li Z, Ma Y, Ma Q, Chen J, Song Y. New perspective on Jun glaze corrosion: study on the corrosion of light greenish blue and reddish purple glazes from Juntai Kiln, Yuzhou, Henan, China. Herit Sci. 2020;8(1):1–11.
60. Ma Q, Xu S, Wang J, Yan J. Integrated analysis of a black-glazed porcelain bowl in Tushan Kiln dated back to Song Dynasty, China. Mater Chem Phys. 2020;242:122213.
61. He Y, Li W, Xu C, Lu X, Sun X. Degradation mechanism of the Ru wares unearthed from the Qingliangsi site in Henan, China. Ceram Int. 2022;48(12):17131–42.
62. He Y, Li W, Li J, Xu C, Lu X. Corrosion of Longquan celadons in the marine environment: Study on the celadons from the Dalian Island shipwreck of the Yuan Dynasty. Herit Sci. 2021;9(1):104.
63. Paul A. Chemical durability of glasses; a thermodynamic approach. J Mater Sci. 1977;12:2246–68.
64. Eppler RA, Eppler DR. Glazes and glass coatings: Amer Ceramic Society; 2000.
65. Liem NQ, Thanh NT, Colomban P. Reliability of Raman micro-spectroscopy in analysing ancient ceramics: the case of ancient Vietnamese porcelain and celadon glazes. J Raman Spectrosc. 2002;33(4):287–94.
66. Colomban PH, Sagon G, Huy LQ, Liem NQ, Mazerolles L. Vietnamese (15th century) blue-and-white, tam thai and lustre porcelains/stonewares: glaze composition and decoration techniques. Archaeometry. 2004;46(1):125–36.
67. Kırmızı B, Chen S, Colomban P. The Raman signature of protonic species as a potential tool for dating or authentication of glazed pottery. J Raman Spectrosc. 2019;50(5):696–710.
68. Colomban P, Ngo A-T, Edwards HG, Prinsloo LC, Esterhuizen LV. Raman identification of the different glazing technologies of blue-and-white Ming porcelains. Ceram Int. 2022;48(2):1673–81.
69. Janssens K. Electron microscopy. In: Janssens K, editor. Modern methods for analysing archaeological and historical glass. London: Wiley; 2013. p. 129–54.
70. Janssens K. X-ray based methods of analysis. In: Janssens K, editor. Modern methods for analysing archaeological and historical glass. London: Wiley; 2013. p. 79–128.
71. Colomban P. Non-destructive raman analysis of ancient glasses and glazes. In: Janssens K, editor. Modern methods for analysing archaeological and historical glass. London: Wiley; 2013. p. 275–300.
72. Gratuze B. Glass characterisation using laser ablation inductively coupled plasma mass spectrometry methods. In: Janssens K, editor. Modern methods for analysing archaeological and historical glass. London: Wiley; 2013. p. 201–34.
73. Kleber C, Schreiner M. Surface analysis. In: Janssens K, editor. Modern methods for analysing archaeological and historical glass. London: Wiley; 2013. p. 247–74.
74. Quartieri S, Arletti R. The Use of X-ray absorption spectroscopy in historical glass research. In: Janssens K, editor. Modern methods for analysing archaeological and historical glass. London: Wiley; 2013. p. 301–9.
75. Zanini R, Roman M, Cattaruzza E, Traviglia A. High-speed and high-resolution 2D and 3D elemental imaging of corroded ancient glass by laser ablation-ICP-MS. J Anal At Spectrom. 2023;38(4):917–26.
76. Colomban P. On-site Raman identification and dating of ancient glasses: a review of procedures and tools. J Cult Herit. 2008;9:e55–60.

77. Colomban P. Rocks as blue, green and black pigments/dyes of glazed pottery and enamelled glass artefacts—a review. Eur J Mineral. 2013;25(5):863–79.
78. Adlington LW, Freestone IC. Using handheld pXRF to study medieval stained glass: a methodology using trace elements. MRS Adv. 2017;2(33–34):1785–800.
79. Simsek G, Unsalan O, Bayraktar K, Colomban P. On-site pXRF analysis of glaze composition and colouring agents of "Iznik" tiles at Edirne mosques (15th and 16th-centuries). Ceram Int. 2019;45(1):595–605.
80. Colomban P, editor The destructive/non-destructive identification of enameled pottery, glass artifacts and associated pigments—a brief overview. Arts; 2013: MDPI.
81. Fischer C, Hsieh E. Export Chinese blue-and-white porcelain: compositional analysis and sourcing using non-invasive portable XRF and reflectance spectroscopy. J Archaeol Sci. 2017;80:14–26.
82. Colomban P, Simsek Franci G, Gironda M, d'Abrigeon P, Schumacher A-C. pXRF data evaluation methodology for on-site analysis of precious artifacts: cobalt used in the blue decoration of Qing Dynasty overglazed porcelain enameled at customs district (Guangzhou), Jingdezhen and Zaobanchu (Beijing) workshops. Heritage. 2022;5(3):1752–78.
83. Yang Z. Several issues about the export of jingdezhen porcelain from the perspective of the porcelain found in ming dynasty shipwrecks in Fujian. In: Jiao T, editor. New research into the maritime trades, seafaring and underwater archaeology of the Ming dynasty: Hong Kong maritime museum international symposium proceedings. Hong Kong: Hong Kong Maritime Museum; 2015. p. 215–41.
84. Chollet H. La porcelaine bleu-et-blanc. In: L'Hour M, editor. La mémoire engloutie de Brunei: précis scientifique. 2. Paris: Textuel; 2001. p. 29–64.
85. Ma H, Zhu J, Henderson J, Li N. Provenance of Zhangzhou export blue-and-white and its clay source. J Archaeol Sci. 2012;39(5):1218–26.
86. Zhu J, Ma H, Li N, Henderson J, Glascock MD. The provenance of export porcelain from the Nan'ao One shipwreck in the South China Sea. Antiquity. 2016;90(351):798–808.
87. Hsieh E, Fischer C. Japanese or Chinese? Non-invasive analysis of East Asian blue-and-white porcelain. Archaeol Anthropol Sci. 2019;11(10):5483–97.
88. Cheng HS, Zhang ZQ, Xia HN, Jiang JC, Yang FJ. Non-destructive analysis and appraisal of ancient Chinese porcelain by PIXE. Nucl Instrum Methods Phys Res Sect B. 2002;190(1–4):488–91.
89. Simsek FG. Handheld X-ray fluorescence (XRF) versus wavelength dispersive XRF: characterization of chinese blue-and-white porcelain sherds using handheld and laboratory-type XRF instruments. Appl Spectrosc. 2020;74(3):314–22.
90. Kerr R, Needham J, Wood N. Science and civilisation in China: volume 5, chemistry and chemical technology, part 12, ceramic technology. Cambridge: Cambridge University Press; 2004.
91. Ma H, Henderson J, Evans J. The exploration of Sr isotopic analysis applied to Chinese glazes: part one. J Archaeol Sci. 2014;50:551–8.
92. De Pauw E, Tack P, Verhaeven E, Bauters S, Acke L, Vekemans B, et al. Microbeam X-ray fluorescence and X-ray absorption spectroscopic analysis of Chinese blue-and-white kraak porcelain dating from the Ming dynasty. Spectrochim Acta, Part B. 2018;149:190–6.
93. Wen R, Wang CS, Mao ZW, Huang YY, Pollard AM. The chemical composition of blue pigment on Chinese blue-and-white porcelain of the Yuan and Ming dynasties (AD 1271–1644). Archaeometry. 2007;49(1):101–15.
94. Bezur A, Casadio F. The analysis of porcelain using handheld and portable X-ray fluorescence spectrometers. In: Shugar AN, Mass JL, editors. Handheld XRF for art and archaeology. Leuven: Leuven University Press; 2012. p. 249–311.
95. Kaiser B, Shugar A. Glass analysis utilizing handheld X-ray fluorescence. In: Shugar AN, Mass JL, editors. Handheld XRF for art and archaeology. Leuven: Leuven University Press; 2012. p. 449–70.
96. Chen Y-c, Kuo Y-y, Chang T-g. An investigation on Chinese blue-and-white ware and its blue pigment. J Chin Ceram Soc. 1978;1978(4):225–41.
97. Cheng HS, Zhang B, Zhu D, Yang FJ, Sun XM, Guo MS. Some new results of PIXE study on Chinese ancient porcelain. Nucl Instrum Methods Phys Res Sect B. 2005;240(1–2):527–31.
98. Ceglia A, Meulebroeck W, Baert K, Wouters H, Nys K, Thienpont H, et al. Cobalt absorption bands for the differentiation of historical Na and Ca/K rich glass. Surf Interface Anal. 2012;44:219–26.
99. Wang T, Zhu T, Feng Z, Fayard B, Pouyet E, Cotte M, et al. Synchrotron radiation-based multi-analytical approach for studying underglaze color: the microstructure of Chinese Qinghua blue decors (Ming dynasty). Anal Chim Acta. 2016;928:20–31.
100. Qu Y, Xu J, Xi X, Huang C, Yang J. Microstructure characteristics of blue-and-white porcelain from the folk kiln of Ming and Qing Dynasties. Ceram Int. 2014;40(6):8783–90.
101. Pinto A, Sciau P, Zhu T, Zhao B, Groenen J. Raman study of Ming porcelain dark spots: probing Mn-rich spinels. J Raman Spectrosc. 2019;50(5):711–9.
102. Roqué-Rosell J, Pinto A, Marini C, Prieto Burgos J, Groenen J, Campeny M, et al. Synchrotron XAS study of Mn and Fe in Chinese blue-and-white Ming porcelains from the second half of the 15th century. Ceram Int. 2021;47(2):2715–24.
103. Colomban PH, Sagon G, Huy LQ, Liem NQ, Mazerolles L. Vietnamese (15th Century) blue-and-white, tam thai and lustre porcelains/stonewares: glaze composition and decoration techniques*. Archaeometry. 2004;46(1):125–36.
104. Donald SB, Swink AM, Schreiber HD. High-iron ferric glass. J Noncryst Solids. 2006;352(6–7):539–43.
105. Möncke D, Papageorgiou M, Winterstein-Beckmann A, Zacharias N. Roman glasses coloured by dissolved transition metal ions: redox-reactions, optical spectroscopy and ligand field theory. J Archaeol Sci. 2014;46:23–36.
106. Kingery WD, Bowen HK, Uhlmann DR. Introduction to ceramics. New York: Wiley; 1976.
107. Fröberg L, Kronberg T, Hupa L. Effect of soaking time on phase composition and topography and surface microstructure in vitrocrystalline whiteware glazes. J Eur Ceram Soc. 2009;29(11):2153–61.
108. Radpour R, Hsieh E, Fischer C. Study of shades and tints of the blue color in export blue-and-white porcelain from late Ming to early Qing dynasty. Poster, ISA conference, Kalamata, Greece; 2016.
109. Jiang X, Ma Y, Chen Y, Li Y, Ma Q, Zhang Z, et al. Raman analysis of cobalt blue pigment in blue and white porcelain: a reassessment. Spectrochim Acta Part A Mol Biomol Spectrosc. 2018;190:61–7.
110. Jiang X, Weng Y, Wu X, Cui J, Lyu H, Jiang J, et al. Early globalized industrial chain revealed by residual submicron pigment particles in Chinese imperial blue-and-white porcelains. Proc Natl Acad Sci. 2020;117(12):6446.
111. Pinto A, Groenen J, Zhao B, Zhu T, Sciau P. Chromogenic mechanisms in blue-and-white porcelains. Journal of the European Ceramic Society; 2020.
112. Kingery WD, Vandiver PB. Ceramic masterpieces: art, structure and technology. New York: The Free Press; 1986.
113. Wen J, Chen Z, Zeng Q, Hu L, Wang B, Shi J, et al. Multi-micro analytical studies of blue-and-white porcelain (Ming dynasty) excavated from Shuangchuan island. Ceram Int. 2019;45(10):13362–8.
114. Zhang R, Garachon I, Gethin P, van Campen J. Double layers glaze analysis of the Fujian export blue-and-white porcelain from the Witte Leeuw shipwreck (1613). Ceram Int. 2020;46(9):13474–81.
115. Zhou Y, Hu Y, Tao Y, Sun J, Cui Y, Wang K, et al. Study on the microstructure of the multilayer glaze of the 16th–17th century export blue-and-white porcelain excavated from Nan'ao-I Shipwreck. Ceram Int. 2016;42(15):17456–65.
116. Simsek G, Colomban P, Wong S, Zhao B, Rougeulle A, Liem NQ. Toward a fast non-destructive identification of pottery: the sourcing of 14th–16th century Vietnamese and Chinese ceramic shards. J Cult Herit. 2015;16(2):159–72.
117. Klein GA. Industrial color physics. Rhodes WT, editor. New York: Springer; 2010.
118. Llusar M, Forés A, Badenes JA, Calbo J, Tena MA, Monrós G. Colour analysis of some cobalt-based blue pigments. J Eur Ceram Soc. 2001;2001(21):1121–30.
119. Peymannia M, Soleimani-Gorgani A, Ghahari M, Najafi F. Production of a stable and homogeneous colloid dispersion of nano $CoAl_2O_4$ pigment for ceramic ink-jet ink. J Eur Ceram Soc. 2014;34(12):3119–26.

120. Tang Q, Zhu H, Chen C, Wang Y, Zhu Z, Wu J, et al. Preparation and characterization of nanoscale cobalt blue pigment for ceramic inkjet printing by sol–gel self-propagating combustion. Mater Res. 2017;20(5):1340–4.
121. Melo DMdA, Cunha JDd, Fernandes JD, Bernardi M, Melo MAdF, Martinelli AE. Evaluation of $CoAl_2O_4$ as ceramic pigments. Mater Res Bull. 2003;38(9–10):1559–64.
122. Serment B, Brochon C, Hadziioannou G, Buffière S, Demourgues A, Gaudon M. The versatile Co^{2+}/Co^{3+} oxidation states in cobalt alumina spinel: how to design strong blue nanometric pigments for color electrophoretic display. RSC Adv. 2019;9(59):34125–35.
123. Ming LZ, Ceramics D. In: Li Z, Bower VL, He L, editors. Chinese ceramics: from the Paleolithic period through the Qing dynasty. New Haven: Yale University Press; 2010. p. 387–458.
124. Du F, Su B. Further study of sources of the imported cobalt-blue pigment used on Jingdezhen porcelain from late 13 to early 15 centuries. Sci China Ser E Technol Sci. 2008;51(3):249–59.
125. Valenstein SG. A handbook of Chinese ceramics. New York: The Metropolitan Museum of Art; 1989.
126. Miksic J, editor. Southeast Asian ceramics: new light on old pottery. Singapore: Editioins Didier Millet; 2010.
127. Trigault N. China in the sixteenth century: the journals of Matthew Ricci, 1583–1610. translated from the Latin by Louis J. Gallagher, S.J. New York: Random House; 1953.

Publisher's Note